Supplementary Information: Morphologically complex environments fundamentally alter dynamics and stability of ecological communities

Nick Lowery and Tristan Ursell
Department of Physics, University of Oregon
Eugene, Oregon USA

1 Calculating Maximum Interface Curvature in a Pillar Array

We assume that all competition boundaries between pillars make right angles with the pillar edges. We also center the system such that we eliminate a parameter and then the equation of the circle of interest is

$$x^2 + (y - y_o)^2 = r^2, \tag{1}$$

where y_o is the y coordinate of the circle of maximum curvature and r is the radius of that circle. We assume that the center-to-center separation of the pillars is Δx and the radius of each pillar is R. We characterize the point of intersection between the pillar edge and the circle of interest by the angle ϕ. Then at the point of intersection (i) between the circle and the pillar the coordinates on the circle are

$$x_i = -\frac{\Delta x}{2} + R\cos(\phi) \tag{2}$$

$$y_i = R\sin(\phi) \tag{3}$$

At that same point the slope of the circle must be equal to $\tan(\phi)$.

The slope is found by taking the implicit derivative

$$\frac{\partial}{\partial x}\left[x^2 + (y - y_o)^2 = r^2\right] \;\rightarrow\; 2x + 2(y - y_o)y_x = 0 \;\rightarrow\; y' = -\frac{x}{y - y_o}, \tag{4}$$

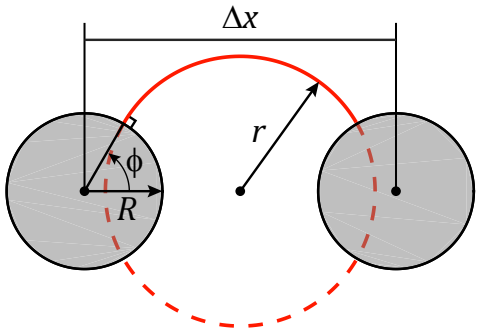

SI Figure 1: Schematic graphically depicting the pillar radius R, pillar separation Δx, and angle ϕ.

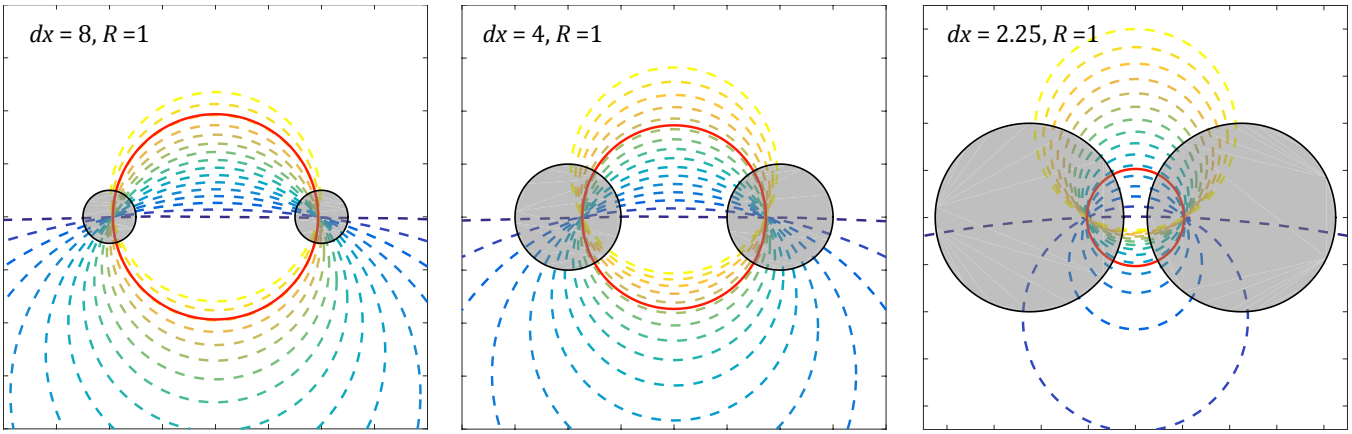

SI Figure 2: Plots of maximum interface curvature as a function of pillar separation. The dashed lines show the interface curvature as a function of the angle (ϕ) from low ϕ (blue) to high ϕ (yellow). The solid red circle shows the circle whose corresponding competitive interface has the highest curvature given the values of R and Δx.

and using this result we can solve for y_o and use that to find r^2

$$\left(\frac{r}{R}\right)^2 = \left(\frac{\delta - \cos(\phi)}{\sin(\phi)}\right)^2 \quad \rightarrow \quad \frac{r}{R} = \frac{\delta - \cos(\phi)}{\sin(\phi)} \tag{5}$$

where the sign ambiguity is irrelevant, and we define $\delta = \frac{\Delta x}{2R}$. Then the minimum radius (maximum curvature) lies at the angle given by

$$\frac{\partial}{\partial \phi}\left(\frac{r}{R}\right) = 0 \quad \rightarrow \quad \phi_c = \tan^{-1}\left(\sqrt{1 - \frac{1}{\delta^2}}, \frac{1}{\delta}\right) \tag{6}$$

where we use the four-quadrant tangent function, and upon substitution

$$\frac{r_{\min}}{R} = \sqrt{\delta^2 - 1} \tag{7}$$

and thus the maximum curvature is

$$\kappa_{\max} = \frac{1}{R\sqrt{\delta^2 - 1}} \tag{8}$$

We note that as $\delta \rightarrow \infty$ the maximum curvature goes to zero and the circle that corresponds to the maximum curvature is the circle whose diameter is Δx. As $\delta \rightarrow 1$ (and hence $\Delta x \rightarrow 2R$) the maximum curvature diverges.

1.1 Relationship to Competitive Asymmetry

We can calculate the maximum possible curvature for a particular lattice with values R and Δx, and if a particular level of competitive asymmetry, $\epsilon = \frac{1}{2}(P_B - P_A)$, requires a higher curvature than this value, the lattice in question will not stably support both species.

We know that such interfaces are flat for symmetric competition ($\epsilon = 0$), while $\epsilon > 0$ results in curved interfaces. Additionally, the sharpness of the competitive interface is inversely related to $\langle P \rangle = \frac{1}{2}(P_A + P_B)$. Thus dimensional arguments demand that the curvature of the competitive interface is set by a function of the dimensionless competition asymmetry, $\epsilon / \langle P \rangle$. The inverse natural length scale of

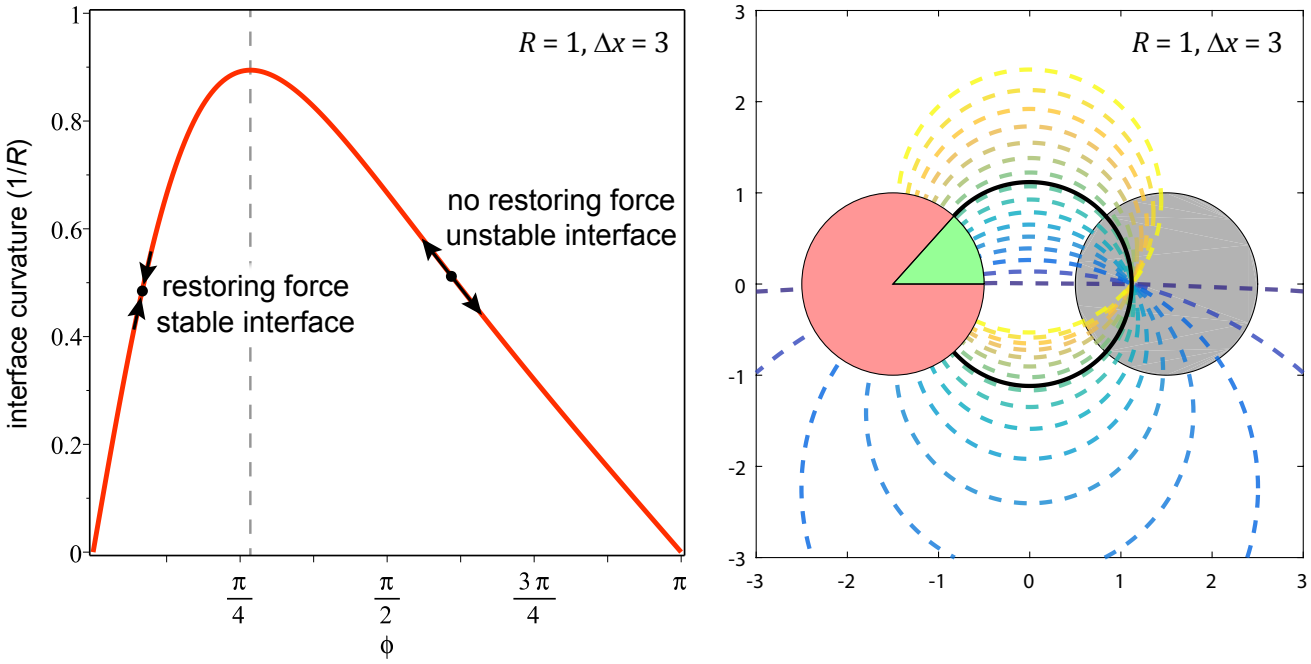

SI Figure 3: (A) Plot of the interface curvature between two pillars with the indicated size and spacing. If the ecologically equilibrated interface curvature is both less than the maximum curvature and lies to the left of the maximum curvature then the dynamics provide a restoring force which stabilizes the interface, otherwise, the interface is unstable. (B) Schematic matched to (A) that shows the zone of stable interface angles ϕ in green (here $0 \leq \phi \lesssim \pi/4$) and unstable zone in red. The end of the green zone and the black circle both correspond to the maximum curvature shown in (A).

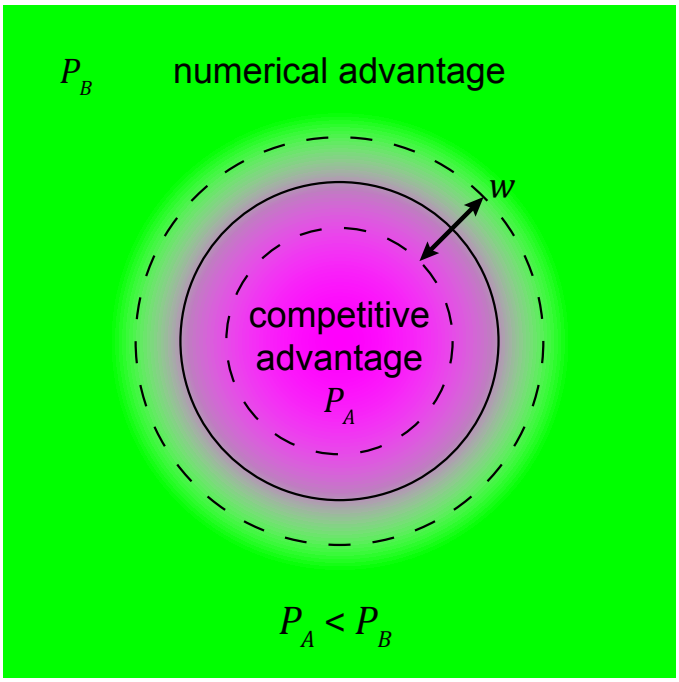

SI Figure 4: A schematic of the unstable equilibrium between two unequal competitors, here with species A (magenta) the stronger competitor (hence $P_A < P_B$). The competition zone has a width w set by the natural length scale $\sqrt{D/r}$. The equilibrium curvature of the competitive interface (solid line) is positioned such that the numerical advantage of the weaker competitor (B) is balanced against the higher potency of the stronger competitor (A).

the system $\frac{1}{\lambda} = \sqrt{r/D}$, sets the natural scale for curvature and thus to within a constant the interfacial curvature in a stable competitive system must be

$$\kappa_{\text{crit}} = \sqrt{\frac{r}{D}} f\left(\frac{\epsilon}{\langle P \rangle}\right). \tag{9}$$

where f is some function. Taylor's theorem then suggests that for a sufficiently smooth function with small dimensionless competitive asymmetries

$$\kappa_{\text{crit}} \propto \frac{\epsilon}{\langle P \rangle}\sqrt{\frac{r}{D}} \tag{10}$$

which is supported by the data in Fig. 2B.

A geometric argument gives similar results; given two strains with unequal competitive fitness, we postulate that at equilibrium (i.e. when the genetic boundary does not move) the ratio of competition parameters P_A and P_B is equal to the ratio of the numeric advantage imposed by a curved interface (as shown in Fig. 4). The width of the transition zone, w, is, to within an order one constant, set by the only natural length scale in the system, $\sqrt{D/r}$, and hence

$$\kappa_{\text{crit}} = \frac{4}{w}\frac{P_B - P_A}{P_B + P_A} \propto \sqrt{\frac{r}{D}}\frac{\epsilon}{\langle P \rangle}. \tag{11}$$

2 Modeling Extinction Time Distributions in Structured Environments

We seek to characterize the classes of dynamics observed during 3-way intransitive competition in our anisotropic environmental simulations. The diagram below shows the states and transition rates between

the three observed dynamical states, with L being limit-cycle (cyclic), C being chaos, and E being extinction. Extinction is a fully absorbing state (hence no arrows emerge from E). The cyclic state is characterized by stable coexistence of all three species and hence the transition rate from L to E is strictly modeled as zero. Our simulations are deterministic and hence for a given initial condition in a particular environment the time course of transitions between these states is encoded by those initial conditions. Thus the ensemble from which we draw trajectories that statistically follow this diagram is the ensemble of random, spatially uncorrelated initial conditions, not a statistical ensemble over stochastic dynamical processes.

2.1 Kinetic Model

We assume that for a given pillar size and spacing, there is a corresponding set of state-transition rates. Over an ensemble of initial conditions, these rates are characterized by the number of observed transitions of a particular type (CL, LC, or CE) per unit time. This model aims to determine the distribution of arrival times into the extinct state and compare those predictions with the simulated distributions. The distribution of arrival times $p(t')$ is related to the extinct ensemble fraction E by

$$dE \propto p(t')dt' \quad \rightarrow \quad p(t') \propto \frac{\partial E}{\partial t'} \tag{12}$$

where the total integrated amount of E is 1 as $t' \rightarrow \infty$ because E is a strictly absorbing state. This means that all trajectories eventually end with extinction, though the time to extinction could be very long if, for instance, specific values of pillar size and spacing result in $k_{LC} \sim 0$, noting that as $\Delta x \rightarrow \infty$, $k_{LC} \rightarrow 0$.

Using this kinetic model, the following ODEs govern the probability of being in each state as a function of time

$$\dot{L} = -k_{LC}L + k_{CL}C \tag{13}$$

$$\dot{C} = k_{LC}L - (k_{CL} + k_{CE})C \tag{14}$$

$$\dot{E} = k_{CE}C \tag{15}$$

Since this describes the time-dependent probability of being in a given state $\dot{L} + \dot{C} + \dot{E} = 0$ and hence the system is conservative. Given that $\dot{E} \propto C$, we note that $C \propto p(t)$ and hence seek to decouple the equations into an equation strictly for C. Solving eqn. 14 for L we find

$$L = \frac{1}{k_{LC}}\left(\dot{C} + (k_{CL} + k_{CE})C\right) \tag{16}$$

and then differentiating with respect to time we find

$$\dot{L} = \frac{1}{k_{LC}}\left(\ddot{C} + (k_{CL} + k_{CE})\dot{C}\right). \tag{17}$$

Then substituting these into eqn. 13 we have

$$\dot{L} = -k_{LC}L + k_{CL}C \quad \rightarrow \quad \frac{1}{k_{LC}}\left(\ddot{C} + (k_{CL} + k_{CE})\dot{C}\right) = -k_{LC}\frac{1}{k_{LC}}\left(\dot{C} + (k_{CL} + k_{CE})C\right) + k_{CL}C \tag{18}$$

which simplifies to

$$\ddot{C} + (k_{LC} + k_{CL} + k_{CE})\dot{C} + k_{LC}k_{CE}C = 0. \tag{19}$$

We note that the two initial conditions that connect to our simulations are $C(0) = C_o$ and $L(0) = L_o$, which then translate into $C(0) = C_o$ and

$$\dot{C}(0) = k_{LC}L_o - (k_{CL} + k_{CE})C_o. \tag{20}$$

In order to reduce the parameter space and reveal natural scales, we non-dimensionalize this equation by choosing the only time scale that behaves well as single $k_{ij} \to 0$, namely

$$t' = t\tau \quad \to \quad \tau = (k_{LC} + k_{CL} + k_{CE})^{-1}. \tag{21}$$

Then switching to the dimensionless t as the time variable, we have

$$\ddot{C} + \dot{C} + KC = 0 \tag{22}$$

with the dimensionless constant

$$K = \frac{k_{LC}k_{CE}}{(k_{LC} + k_{CL} + k_{CE})^2}. \tag{23}$$

The rate constants are all positive, $k_{ij} \geq 0$, and hence it can be shown that

$$0 < K < \frac{1}{4} \tag{24}$$

for all values of k_{ij}[1]. This also transforms the initial condition to

$$\dot{C}(0) = \tau\left(k_{LC}L_o - (k_{CL} + k_{CE})C_o\right) = \tau k_{LC}L_o + (\tau k_{LC} - 1)C_o. \tag{25}$$

2.1.1 Initial Condition $C(0) = 0$ $L(0) = 1$

There are two solutions of interest, namely when $(C_o, L_o) = (0, 1)$ and $(C_o, L_o) = (1, 0)$. Any other initial condition is a linear combination of these two solutions. Let us examine $(C_o, L_o) = (0, 1)$, which has the solution

$$C(t) = \tau k_{LC}\frac{e^{-\frac{t}{2}}}{\alpha}\sinh(\alpha t) \tag{26}$$

with $\alpha = \frac{\sqrt{1-4K}}{2}$. Then building on the fact that $\dot{E} = k_{CE}C = p(t)$

$$p_{01}(t) = \dot{E} = \tau k_{CE}C(t) = \frac{K}{\alpha}e^{-\frac{t}{2}}\sinh(\alpha t) \tag{27}$$

where the factor of τ comes from the non-dimensionalization and the subscript 01 in p refers to the initial conditions used to derive this version of p. On long time scales

$$\int_0^\infty p_{01}(t)\mathrm{d}t = \frac{K}{\alpha}\int_0^\infty e^{-\frac{t}{2}}\sinh(\alpha t)\,\mathrm{d}t = \frac{\frac{1}{4} - \alpha^2}{\alpha}\int_0^\infty e^{-\frac{t}{2}}\sinh(\alpha t)\,\mathrm{d}t = 1 \tag{28}$$

for all values of $0 < \alpha < \frac{1}{2}$, meaning all trajectories lead to the fully absorbing state of extinction.

2.1.2 Initial Condition $C(0) = 1$ $L(0) = 0$

Examining $(C_o, L_o) = (1, 0)$, combining terms and simplifying, this has the solution

$$C(t) = \frac{e^{-\frac{t}{2}}}{2\alpha}\left[2\alpha\cosh(\alpha t) + (2\tau k_{LC} - 1)\sinh(\alpha t)\right] \tag{29}$$

and then $p_{10}(t) = \dot{E} = \tau k_{CE}C(t)$ and hence

$$p_{10}(t) = \frac{K}{\alpha}e^{-\frac{t}{2}}\sinh(\alpha t) + \gamma\frac{e^{-\frac{t}{2}}}{2\alpha}\left[2\alpha\cosh(\alpha t) - \sinh(\alpha t)\right] \tag{30}$$

[1] Examining $K' = \frac{ab}{(a+b)^2}$, which is maximized when $a = b$ and hence $K' = \frac{1}{4}$. Then changing to $K'' = \frac{ab}{(a+b+c)^2}$ with $c > 0$ and hence $0 < K'' \leq K'$.

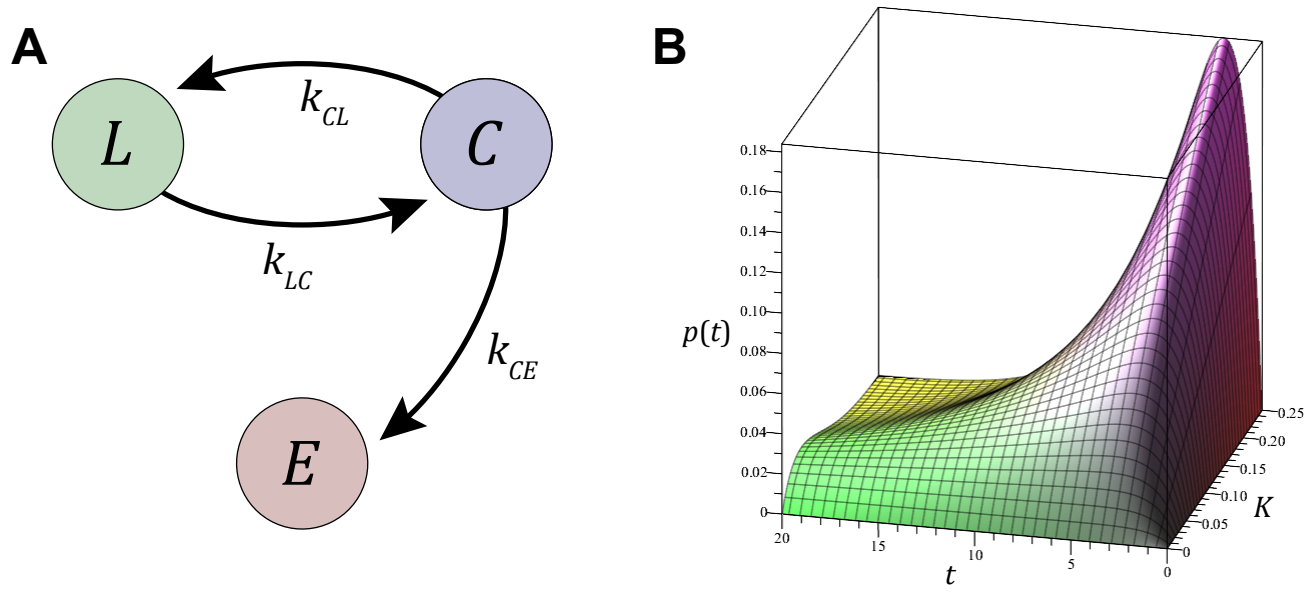

SI Figure 5: (A) Schematic showing dynamical states (limit-cycle / cyclic L, chaotic C, and extinct E) and the mean rates of transition that connect them. (B) The family of extinction time distributions as a function of dimensionless time and the dimensionless rate parameter K for $C(0) = 0$ and $L(0) = 1$ that result from the kinetic model in (A).

with

$$\int_0^\infty p_{10}(t)\mathrm{d}t = 1. \tag{31}$$

The dimensionless constant $\gamma = \tau k_{CE}$ is bounded to be $0 < \gamma < 1$. We note that the first term in the above equation is the solution for $p_{01}(t)$ that we found for $C(0) = 0$ and $L(0) = 1$, that solution integrates to one and hence that demands that

$$\int_0^\infty e^{-\frac{t}{2}} \left[2\alpha \cosh(\alpha t) - \sinh(\alpha t)\right] \mathrm{d}t = 0, \tag{32}$$

which it does. Then we note that both γ and K are functions of k_{ij} and hence are not fully independent parameters. Examining the structure of K and γ, first we note that

$$K = \frac{k_{LC}}{k_{CE}}\gamma^2 \tag{33}$$

and that the maximum value of γ is when $k_{CL} = 0$ and thus as a function of k_{LC} and k_{CE}, the maximum value of γ is

$$\gamma = \frac{1}{1 + \frac{k_{LC}}{k_{CE}}} \quad \rightarrow \quad \gamma = \frac{1}{1 + \frac{K}{\gamma^2}} \tag{34}$$

Thus the maximum value of K is bounded by

$$K \leq \gamma(1 - \gamma) \tag{35}$$

and the minimum is zero. Any arbitrary (arb) initial condition is a weighted sum of these two solutions for the extinction probability

$$p_{\mathrm{arb}} = (1 - f)p_{01}(t) + f p_{10}(t) \tag{36}$$

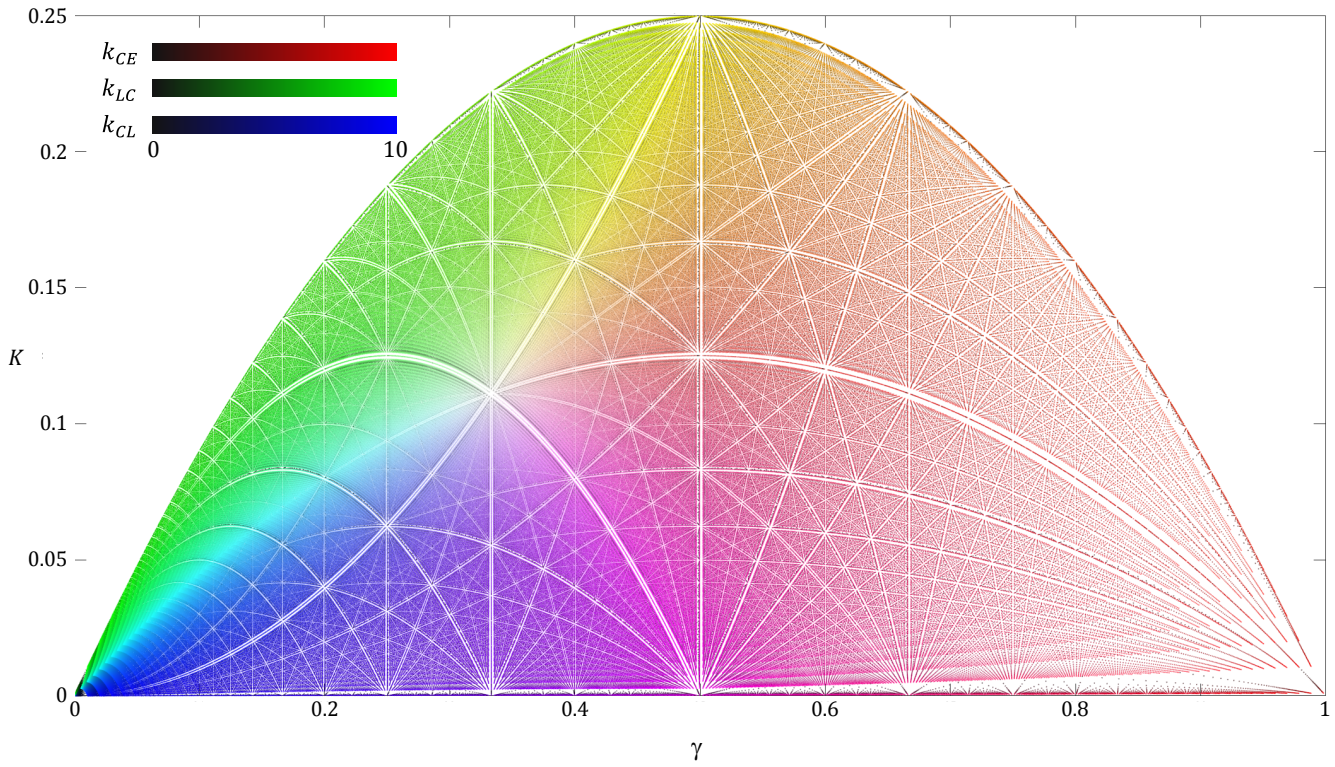

SI Figure 6: The two dimensionless rate parameters K and γ are not fully independent of each other because they are both functions of k_{ij} and $k_{ij} > 0$. As shown in this text, $K \leq \gamma(\gamma - 1)$, here shown by the bounding parabola, where the values within that region are fractally organized. We do not yet know the full mapping from this kinetic parameter space to the morphological space specified by R and Δx.

with $0 < f < 1$ being the weighting. Then because p_{01} and p_{10} share terms this simplifies to

$$p_{\text{arb}}(t) = \frac{K}{\alpha} e^{-\frac{t}{2}} \sinh(\alpha t) + f\gamma \frac{e^{-\frac{t}{2}}}{2\alpha} \left[2\alpha \cosh(\alpha t) - \sinh(\alpha t)\right]. \tag{37}$$

While we know that K and γ obey $K \leq \gamma(1-\gamma)$, f is an independent parameter.

Examining our simulations, the fit parameters to the output distributions have a wide range of K, given that $0 < K < 1/4$, suggesting that $\gamma \sim \frac{1}{2}$ for most simulations and hence that $k_{CE} \sim k_{CL} + k_{LC}$. Likewise, we found that fitting bounded $f \ll 1$. This parameter regime suggests that simulations tend to start off in the limit-cycle phase and migrate to the chaotic phase before going extinct. In fitting the extinction time distributions, we fit for both K and τ, ignoring γ because $f \ll 1$, and we allowed for a small time translation $t \to t - t_o$ to account for the 'grow-in' period from random initial conditions.

3 Classification of Dynamic States

4 Extinction Dynamics in Asymmetric Lattices

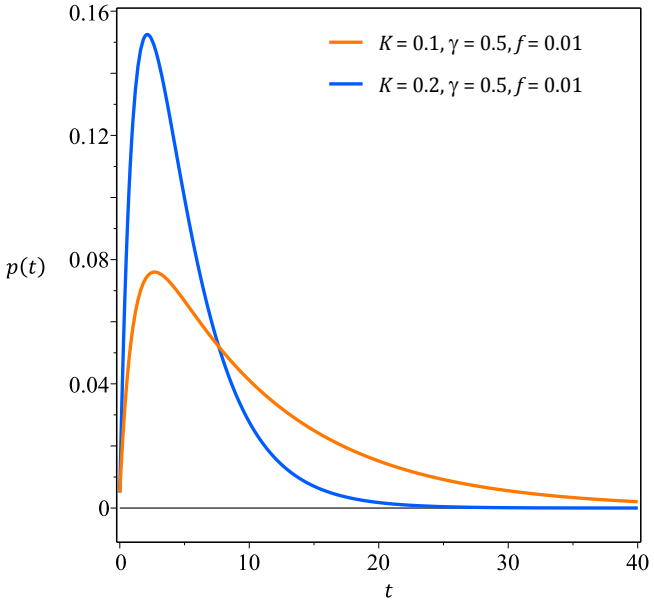

SI Figure 7: Examples of the extinction time distributions for different values of K, γ, and f that resemble what we see from our simulations.

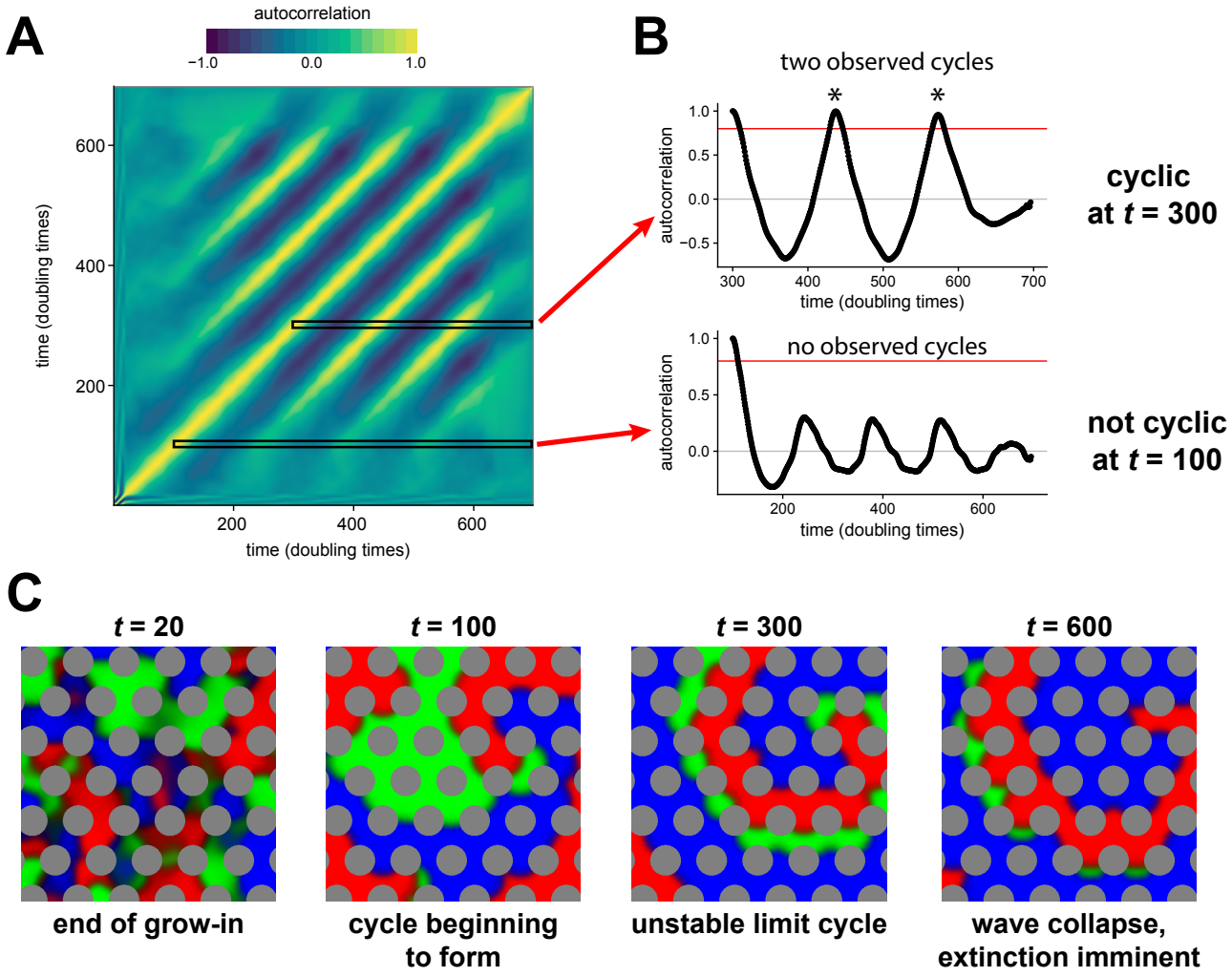

SI Figure 8: Classification of intransitive community dynamics. (A) For every simulation, the temporal autocorrelation was calculated using the vectorized pixel intensities of all species for every non-pillar pixel in the system. (B) The resulting autocorrelation matrix was then used to determine if the spatial distributions of species recapitulated themselves to a sufficiently high degree for at least two cycles; if so, the simulation was classified as cyclic at that time point. A threshold correlation of 0.8 was chosen (red line), as this was the level at which isotropic simulations were reliably classified as cyclic over the entire simulation (excluding grow-in and time points fewer than two cycles from the end of the simulation). The resulting time-dependent classifications were used to generate Figure 5A. The data for this figure was taken from a simulation with $L/(1.29\lambda) = 100$, $P = 0.1$, $R/(1.29\lambda) = 6$ and $\Delta x = 3R$. (C) Snapshots of this simulation corresponding to distinct dynamic regimes. After a short grow-in period, the simulation relaxed into a limit cycle driven by a single wave center about one of the pillars (right upper-middle at $t = 100$ and 300). This wave center was unstable (note asymmetric species distributions about the pillar at $t = 100$ and 300 and wave widths at $t = 300$), persisting for several hundred doubling times until collapse of the wave center resulted in an extinction cascade at $t = 700$ (trivial autocorrelations of the victorious monoculture that persisted until the end of the simulation are not included in the analysis).

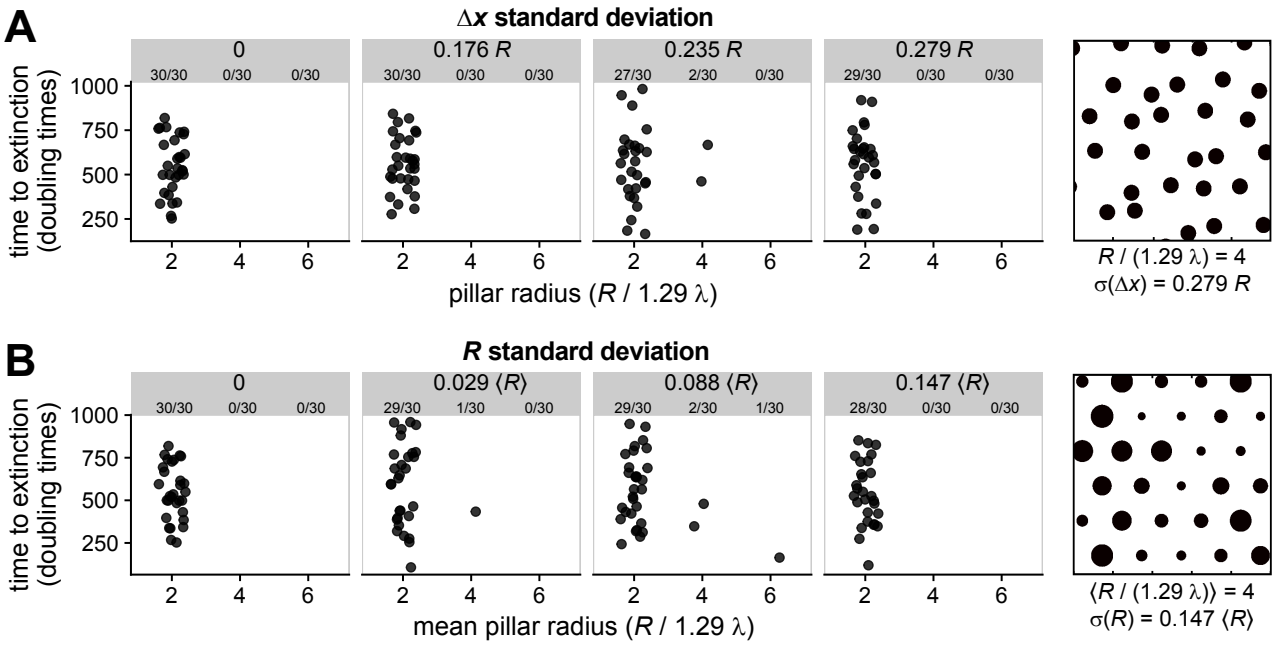

SI Figure 9: Randomized pillar arrays do not affect qualitative community outcomes. Pillar arrays were randomized by drawing (A) pillar spacing (Δx) or (B) pillar radius (R) from a uniform distribution of varying width. In (A) pillar positions were randomized by jittering pillar positions, with the displacement direction chosen randomly and the displacement magnitude drawn from a uniform distribution with mean $5R$ and standard deviation as indicated in panel headings. In (B) the positions remained symmetric but the pillar radii varied, drawn from a uniform distribution with the indicated mean and variance. Example randomized arrays are shown at right. For each standard deviation, three independent realizations of the jittered grid of pillars were generated and manually validated to ensure pillars were not overlapping or spaced too closely for the accurately simulate diffusion. Ten random initial condition replicates were performed for each of the three grids, giving 30 total simulations for each standard deviation in Δx or R. Fractions within subheadings of each panel indicate the observed frequency of extinction for each condition. In all cases, extinction frequency did not show a significant dependence on the standard deviation of Δx nor R, whereas extinction frequency showed a strong dependence on mean lattice parameters, consistent with observations in the main text. Plotted points are jittered along the x-axis to reduce overlap. Simulation parameters are $L/(1.29\lambda) = 100$ and $P = 0.1$, with indicated pillar radius R and spacing $\Delta x = 5R$ before addition of random variation as indicated.